Journal of Sound and Vibration (2001) **246**(2), 245–263
doi:10.1006/jsvi.2001.3628, available online at http://www.idealibrary.com on IDEAL®

ACOUSTIC RADIATIONS FOR SUBMERGED ELASTIC STRUCTURES USING NATURAL MODE EXPANSIONS IN CONJUNCTION WITH RADIATION MODES APPROACH

P.-T CHEN

Department of System Engineering and Naval Architecture, National Taiwan Ocean University, 2 Pei Ning Road, Keelung 202, *Taiwan, Republic of China. E-mail: ptchen@sena.ntou.edu.tw*

(*Received* 28 *September* 2000, *and in final form* 3 *January* 2001)

This work formulates submerged elastic structures using *in-vacuo* vibrational mode expansions with which the acoustic impedance loading is derived based on radiation mode theory. The displacement of natural modes on the normal direction is expanded as linear combinations of a set of velocity radiation modes that the expansion coefficients characterize as the radiation characteristics of each vibration mode. This type of expansion allows one to represent the surface pressure by the corresponding set of pressure radiation modes. Thus, a symmetric impedance matrix associated with the natural vibration mode expansions is derived when a variational increment is applied to the virtual work done by the surface pressure against the normal displacement. The equation of the submerged structures is obtained according to Hamilton's principles. By incorporating the description of radiation modes, this equation of natural mode expansions is used to study the coupling among vibration modal amplitudes due to the modal cross-impedances and the convergence of near and farfield solutions. In addition, a slender submerged spheroidal shell vibrating axisymmetrically serves as a numerical example to demonstrate the effectiveness of the analysis procedure. This numerical example reveals that the acoustic impedances decrease with ascending mode numbers, causing the high order vibration modes to react independently. Moreover, the convergence of the surface pressure and normal velocity is examined on the basis of independent reaction of the vibration modes. Accurately predicting farfield solutions depends only on the convergence of the surface quantities whose components pertain to strong radiation modes. The numerical example indicates that the number of vibration modes used in the expansion for predicting farfield solutions is less than the modes required for the surface solution.

1. INTRODUCTION

Responses of submerged structures depend on the coupled interactions of structural vibrations and fluid loadings. A conventional means of handling structural equations is to express the structural vibrations as the linear superposition of *in-vacuo* natural vibrational modes. An acoustic radiation impedance matrix, in which the surface pressure and normal velocity of the wetted surface are related, can describe acoustic loading. The coupling condition of structures with acoustic loading inquires into the continuity of the structural normal velocity with the acoustic particle normal velocity. Such an approach has received considerable attention, particularly in terms of investigating fluid–structural interaction problems (see references [1–6]).

Our earlier work [7] formulated the equation of submerged structures in such a manner that the solved coefficients of the equation are directly related to the description of acoustic

0022-460X/01/370245 + 19 $35.00/0

radiation. The equation is formulated by selecting the normal displacement of the wetted surface as the equation variable where the displacement variables other than the normal one are eliminated by expressing these variables as a function of the normal displacement. The connection of the normal velocity with acoustic radiation is established as the equation is transformed into a generalized co-ordinate system using a set of velocity radiation modes as a basis. The derivation of the radiation modes was based on a surface acoustic reciprocity which is valid for the linear acoustics of non-viscous medium. The body is immersed in an infinite extend medium. Since the radiation modes manifest either radiating power into far-fields or production of an evanescent field near the surface [8], the modal amplitudes of the radiation modes thus reflect the radiation characteristics of the submerged elastic structures.

In light of the above discussion, this work formulates structural acoustic problems in terms of *in-vacuo* natural vibrational modes by incorporating the radiation mode theory that the structural responses are directly related to radiation characteristics. An acoustic loading matrix is derived based on the surface pressure and normal velocity expansions in terms of pressure and velocity radiation modes. As is well known, an evanescent field caused by a vibrating surface does not propagate acoustic power into the farfield. The surface responses can be characterized either as the component producing only an evanescent field or the component radiating acoustic pressure into the farfield [8]. Analysis is performed of the coupling of the vibrational modal amplitudes due to the acoustic loading and the associated radiation characteristics of the vibrational modes on the basis of the radiation mode theory. This analysis is further applied to explore the convergence of the natural mode expansions to the solutions of surfaces and farfields.

2. FORMULATION OF SUBMERGED STRUCTURES

The potential and kinetic energies of an axisymmetrically submerged shell structure under axisymmetric vibrations can be represented in terms of natural mode expansions [9]

$$V = \frac{1}{2} Eh_0 a^2 \sum_{i=1}^{N_s} (\Delta_i a)^2 \left(\frac{c_0}{c_d}\right)^2 q_i^2,$$

$$T = \frac{1}{2} \rho_s h_0 a^4 \sum_{i=1}^{N_s} \dot{q}_i^2. \tag{1}$$

The symbols used in equations are listed in Appendix A. The factors Eh_0a^2 and $\rho_s h_0 a^4$ are derived from a non-dimensionalized derivation. The surface normal displacement is superposed by the natural modes.

$$w_n = a \sum_{i=1}^{N_s} q_i \phi_{n,i}. \tag{2}$$

The virtual work due to the surface pressure and an external point force f_0 against the normal displacement is then expressed as

$$\delta W = -\int_S \rho_0 c_0^2 \, p\delta \left(a \sum_{i=1}^{N_s} q_i \phi_{n,i} \right) \mathrm{d}S + f_0 \delta \left(a \sum_{i=1}^{N_s} q_i \, \phi_{n,i}^* \right). \tag{3}$$

The surface pressure can be related to the normal velocity using radiation mode theory which has been presented in the previous studies [7, 8]. According to equation (2), the

normal velocity is

$$v_n = c_0 \sum_{i=1}^{N_s} (-\mathrm{i}ka) q_i \phi_{n,i}. \tag{4}$$

where the factor $-\mathrm{i}ka$ represents non-dimensionalized time derivative so that the mono-frequency oscillation time factor is taken as $\mathrm{e}^{-\mathrm{i}\omega t}$. Here, the symbol '$i$' in the subscript denotes the summation index; otherwise, it represents the imaginary value $\sqrt{-1}$ hereinafter. Let the mode shape on the normal direction $\phi_{n,i}$ be expanded as a linear combination of velocity radiation modes Φ_j:

$$\phi_{n,i} = \sum_{j=1}^{N_f} \beta_{ij} \Phi_j, \quad i = 1, 2, \ldots, N_s. \tag{5}$$

The combination coefficients β_{ij} can be computed using the bi-orthogonal condition of pressure radiation modes Ψ_j and velocity radiation modes Φ_j [7, 8], which is

$$\int_s \Phi_i \Psi_j \, \mathrm{d}S = \delta_{ij} \sqrt{\lambda_j^2 + 1}. \tag{6}$$

Details of the radiation mode theory can be found elsewhere [8]. Consequently, the coefficients β_{ij} are identified as

$$\beta_{ij} = \frac{\int \phi_{n,i} \Psi_j \, \mathrm{d}S}{\sqrt{\lambda_j^2 + 1}}. \tag{7}$$

The values of β_{ij} represent the participation factors of the velocity radiation modes Φ_j, $j = 1, 2, 3, \ldots$ to the wetted surface of the nth structural mode $\phi_{n,i}$. Since the radiation modes are derived based on the radiation capabilities so that the lowest order refers to the most efficient radiator, the coefficients of β_{ij} indicate the capability of a nature mode radiating acoustic power to the farfield (see Figure 1). Substituting equations (7) and (5) into equation (4) leads to the expression of surface normal velocity as a linear combination of the velocity radiation modes Φ_j,

$$v_n = c_0 \sum_{j=1}^{N_f} \left(\sum_{i=1}^{N_s} -\mathrm{i}ka q_i \beta_{ij} \right) \Phi_j. \tag{8}$$

Correspondingly, the surface pressure is [7, 8]

$$\rho_0 c_0^2 \, p = \rho_0 c_0^2 \sum_{j=1}^{N_f} \left(\sum_{i=1}^{N_s} -\mathrm{i}ka q_i \beta_{ij} \right) \frac{\lambda_j - i}{\sqrt{\lambda_j^2 + 1}} \Psi_j, \tag{9}$$

where the factor $(\lambda_j - i)/\sqrt{\lambda_j^2 + 1}$ denotes a phase shift of the complex amplitude of pressure radiation mode Ψ_j with respect to the complex amplitude of velocity radiation mode Φ_j.

The above expansions of surface quantities into respective radiation modes are valid for the classical linear acoustic equations, that is, the linearized mass conservation, Euler's equation, and adiabatic state equation. Specifically, the reciprocal principle for surface acoustics, which is the foundation of the radiation mode theory [8], is true under the conditions that,

$$\rho_0 \mathrm{i}\omega \mathbf{v} = \nabla p, \qquad \frac{1}{c_0^2}, \mathrm{i}\omega p = \rho_0 \nabla \cdot \mathbf{v}, \tag{10}$$

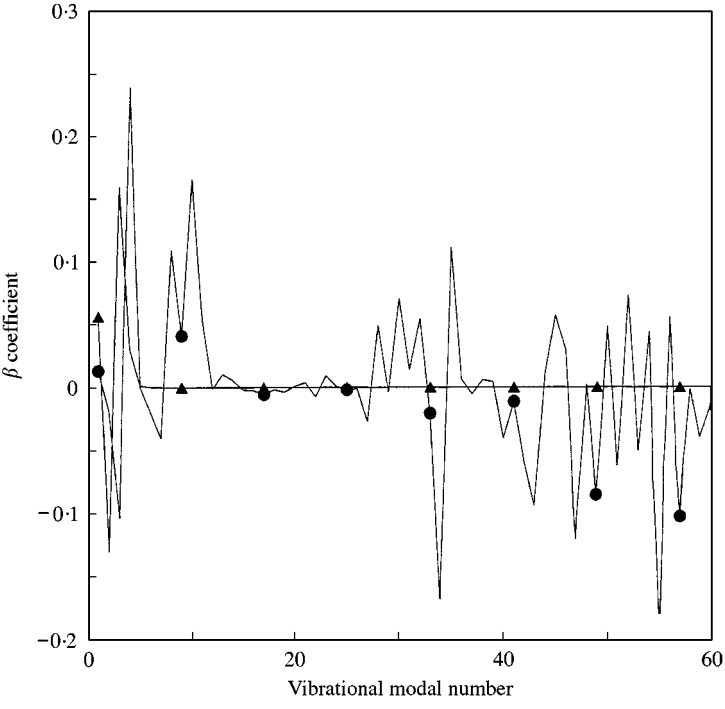

Figure 1. Expansion coefficients β_{ij} of the normal displacement of the first and 10th vibrational *in-vacuo* modes: —▲—, first natural mode; —●—, 10th natural mode.

where the first equation is a linearized Euler's equation and the second equation is a linearized mass conservation with the adiabatic state equation. In equation (10), $\mathbf{v}$ and p denote particle velocity and field pressure respectively. For the situation of viscous fluid, the linearized acoustic equation has to account for viscosity in the momentum equation as well as a thermodynamic process, which is not an adiabatic process, making the expressions of equation (10) complicated [10]. Thus, the modification of the radiation modes to include viscosity is not an obvious derivation and it is hard to assert at the present stage the existence of radiation modes for viscous fluid.

Substituting equations (9) and (5) into equation (3) and using the bi-orthogonal condition, equation (6), lead the virtual work to

$$\delta W = -\rho_0 c_0^2 a^3 \sum_{j=1}^{N_f} \sum_{\ell=1}^{N_s} \sum_{i=1}^{N_s} -\mathrm{i}ka\beta_{\ell j}\beta_{ij}(\lambda_j - i)\, q_i\, \delta q_\ell + f_0 \delta \left(a \sum_{\ell=1}^{N_s} q_\ell \phi^*_{n,\ell} \right). \tag{11}$$

The equation of motion emerges when one applies Hamilton's principles

$$\delta \int_1^2 (T - V)\, \mathrm{d}t + \int_1^2 \delta W\, \mathrm{d}t = 0, \tag{12}$$

which leads to

$$\rho_s h_0 a^4 \ddot{q}_\ell + E h_0 a^2 \left(\frac{c_0}{c_d} \right)^2 (k_\ell a)^2 q_\ell + \rho_0 c_0^2 a^3 (-\mathrm{i}ka) \sum_{j=1}^{N_f} \sum_{i=1}^{N_s} q_i \beta_{ij} (\lambda_j - i)\, \beta_{\ell j} = f_\ell.$$

$$\ell = 1, 2, \ldots, N_s, \tag{13}$$

where the generalized force f_ℓ is defined as

$$f_\ell = af_0\, \phi^*_{n,\ell}. \tag{14}$$

Divide equation (12) by $\rho_0 c_0^2 a^3$ and use the identity $c_d = (E/\rho_s)^{1/2}$ to make the equation dimensionless:

$$\left(\frac{\rho_s}{\rho_0}\right)\left(\frac{h_0}{a}\right)[-(ka)^2 + (\Delta_\ell\, a)^2]\, q_\ell + (-\mathrm{i}ka) \sum_{j=1}^{N_f} \sum_{i=1}^{N_s} q_i \beta_{ij} (\lambda_j - i)\, \beta_{\ell j} = \hat{f}_\ell, \quad \ell = 1, 2, \ldots, N_s, \tag{15}$$

where $\hat{f}$ is the corresponding dimensionless generalized force, and $\ddot{q}_i$ has been substituted by $-\omega^2 q_i$ for mono-frequency oscillation. Write the above equation into a matrix notation.

$$[\Lambda]\{q\} + (-\mathrm{i}ka)[Z]\{q\} = \{\hat{f}\}, \tag{16}$$

in which the matrix $[\Lambda]$ is a diagonal matrix with elements $(\rho_s/\rho_0)\,(h_0/a)\,[-(ka)^2 + (k_\ell\, a)^2]$ and $[Z]$ is a symmetric complex impedance matrix whose elements are

$$Z_{i\ell} = \sum_{j=1}^{N_f} \beta_{ij}\beta_{\ell j}\,(\lambda_j - i). \tag{17}$$

The impedance $Z_{i\ell}$ for i not equal to ℓ is referred to as a cross-coupling impedance for the modes $\phi_{n,i}$ and $\phi_{n,\ell}$, and is a self-coupling impedance for i equal to ℓ. It is instructive to example the acoustic impedance matrix in terms of surface complex acoustic powers. Let $c_0\phi_{n,i}$ be the surface velocity distribution conformable to the profile of $\phi_{n,i}$ which has the velocity radiation mode expansions presented in equation (5). The corresponding surface pressure arising from the normal velocity $c_0\,\phi_{n,i}$, denoted as $\rho_0 c_0^2 p_i$, can be identified, by referring to equation (4), as that one lets the velocity amplitude $-\mathrm{i}kaq_i$ associated with $\phi_{n,i}$ to be unity and other modes to be zero. Examining equations (8) and (9) leads to

$$p_i = \sum_{j=1}^{N_f} \beta_{ij} \frac{\lambda_j - i}{\sqrt{\lambda_j^2 + 1}}\, \Psi_j. \tag{18}$$

Correspondingly, the surface complex acoustic power $\rho_0 c_0^3 P_{ii}$ due to the surface quantities $c_0\phi_{n,i}$ and $\rho_0 c_0^2 p_i$ is the surface integral of the product of the two quantities. Applying the bi-orthogonal condition of Φ_i and Ψ_j in equation (6) leads to

$$P_{ii} = \frac{1}{2} \sum_{j=1}^{N_f} \beta_{ij}\beta_{ij}\,(\lambda_j - i). \tag{19}$$

The coupling surface complex power $\rho_0 c_0^3 P_{i\ell}$ for i not equal to ℓ arises when one considers the product of surface pressure $\rho_0 c_0^2 p_i$ generated by the velocity $c_0\phi_{n,i}$ with the complex conjugate of normal velocity $c_0\phi_{n,\ell}$, which is

$$P_{i\ell} = \frac{1}{2} \sum_{j=1}^{N_f} \beta_{ij}\beta_{\ell j}\,(\lambda_j - i). \tag{20}$$

Equations (18) and (19) are identical to the definition of equation (16) except for a factor of one-half, which indicates that the acoustic loading term in equation (15) is equivalent to the

radiation impedance. The correlation of the acoustic impedance matrix and surface complex power is further examined in the following section.

3. NUMERICAL EXAMPLES OF MODAL IMPEDANCES FOR A SLENDER SPHEROIDAL SHELL

In this section, we demonstrate the preceding formulation using a slender spheroidal shell whose aspect ratio of major axis to minor axis a is four, and the thickness ratio of major radius to the minor radius is 0·02. The material constants are that the ratio of dilatational wave speed to sound speed c_0 is 3·386, the ratio of shell density to fluid density is 7·9, and the Poisson ratio of the shell is 0·3. The shell vibrates axisymmetrically. The shell's dynamic equation based on the classical thin shell theory is formulated using Hamilton's principles incorporated with the displacement variables expanded by assumed mode expansions. A detailed derivation can be found elsewhere [9]. A set of natural vibrational modes is obtained by an eigenvalue problem analysis. Radiation mode analysis is performed by considering surface acoustic power in which selecting velocity and pressure radiation modes makes the complex power a diagonal representation [7]. Each radiation mode reacts independently. Two point loads $\pi\rho_0 c_0^2 a^2$ are applied at the two apexes of the shell vibrating at the dimensionless frequency ka 1·8.

Figure 1 presents the β_{ij} coefficients of the first natural mode and an arbitrarily selected 10th mode where only the integer values are meaningful on the vibration modal numbers. This figure reveals that the lower order natural modes, which are selected as the first mode for demonstration, contain lower order radiation modes. Meanwhile, the higher order natural modes, in which the 10th mode is selected for illustration, exhibit more components on high order radiation modes. As mentioned earlier, the real part of equation (18) denotes the radiated power caused by the normal velocity $c\phi_{n,i}$, where the summation with respect to the index j in equation (18) represents the contribution due to the jth radiation mode Φ_j. The first few non-zero eigenvalues values at ka equal to 1·8 are 3·36, 2·18, 0·88, and 0·09, and the rest are nearly zero. The detailed derivation can be found in the literature [8]. It was pointed out in literature that the magnitude of each eigenvalue indicates the effectiveness of radiating acoustic power to the farfield of that radiation mode. The set of radiation modes is categorized into strong and weak radiation modes based on the magnitude of eigenvalues. The present numerical example shows only the first four radiation modes to be strong radiators. Consequently, Figure 1 reveals that the first natural mode provides more effective power radiation than the 10th order natural mode due to more significant components on the lower order radiation modes for the first natural mode. A close examination of the coefficients β_{ij}, which are not displayed herein, indicates that the lower order vibrational modes generally exhibit more effectiveness in radiating power, while the higher order modes provide more reactive powers, subsequently producing evanescent fields.

Figure 2 plots the magnitude of the dimensionless impedance matrix $Z_{i\ell}$, which is divided by $\rho_0 c_0$, at ka equal to 1·8. Only the values at the integer vibrational mode numbers are meaningful, whereas the interpolated surface other than the integer points is only for a better visualization. This figure also reveals that the self-impedances Z_{ii} are generally larger than the cross-impedances $Z_{i\ell}$ for a given modal number i. In addition, the impedances approach zero values with increasing modal numbers. Figure 3 plots the magnitudes and phases of the self-impedances versus mode numbers, which presents the decreasing of the impedances with the phases approaching 90° as mode numbers become large. This phenomenon reflects the acoustic loading on the natural vibration modes

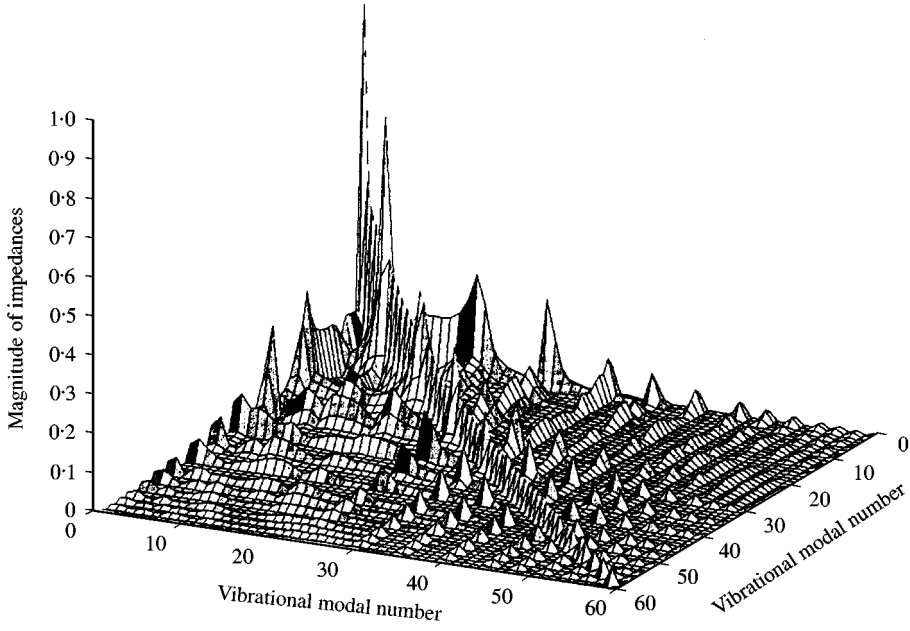

Figure 2. Magnitudes of the impedance matrix versus vibrational modal numbers of the spheroidal body at $ka = 1{\cdot}8$.

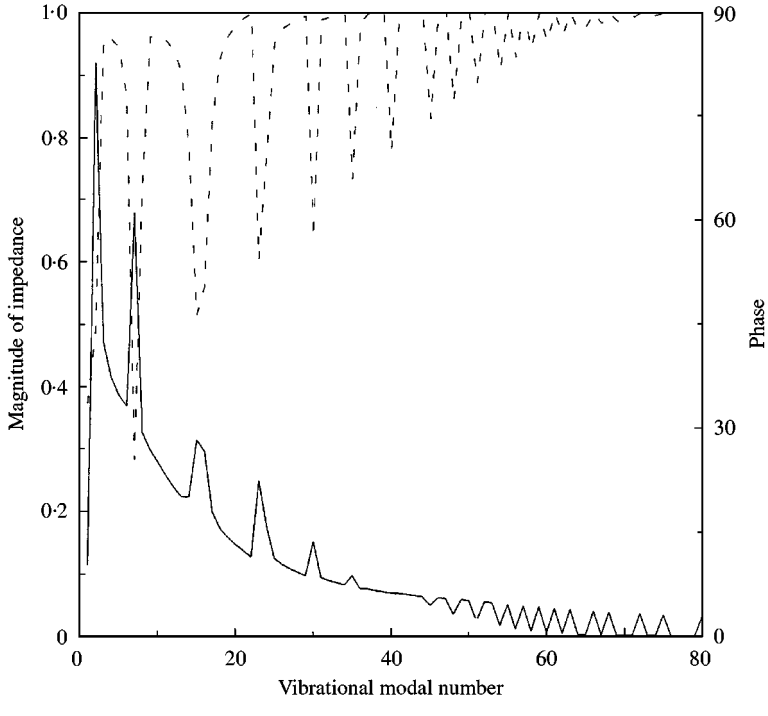

Figure 3. The magnitudes and phases of the self-impedance versus vibrational modal numbers of the spheroidal body at $ka = 1{\cdot}8$.

becoming mass-like effects for relatively high order vibration modes while the loading tends to be absent for high order modes.

4. NUMERICAL DEMONSTRATIONS OF THE COUPLED EQUATION FOR SUBMERGED STRUCTURES

The coupled equation for the submerged structure is formed by equation (15) where the structural inertia and stiffness effects are represented by the diagonal matrix $[\Lambda]$. Meanwhile, the acoustic complex impedance matrix $[Z]$ product of the dimensionless frequency factor $-\mathrm{i}ka$ represents the acoustic loading. Obviously, the modal amplitudes $\{q\}$ are coupled to each other due to the cross-impedances. Figure 4 plots dynamic stiffness matrix $[\Lambda] + (-\mathrm{i}ka)[Z]$ of the spheroidal shell, where the upper subplot shows the stiffness from the first to 10th modes for a more detailed illustration. Again, only the integer values on the vibrational modal numbers are meaningful. According to this figure, the structural inertia and stiffness effects increasingly predominate the acoustic loading when mode numbers increase. This phenomenon is also observed in Figure 2, indicating that the values of the impedances decrease with the ascendant mode numbers while the corresponding structure dynamic stiffnesses become large. Figure 5 shows the vibrational modal amplitudes solved by equation (15), where the numbers of truncated natural vibrational modes used to form equation (15) are chosen as 10, 20, 30 and 80 modes respectively. The amplitudes obtained by using 80 expansion modes are convergent because they approach zero when modes tend towards large numbers. Comparing the solved amplitudes for using the various numbers of natural modes reveals that the modal amplitudes for using 20, 30, and 80 mode expansions at low order vibrational mode numbers are virtually identical and there is some discrepancy for using 10 mode expansions.

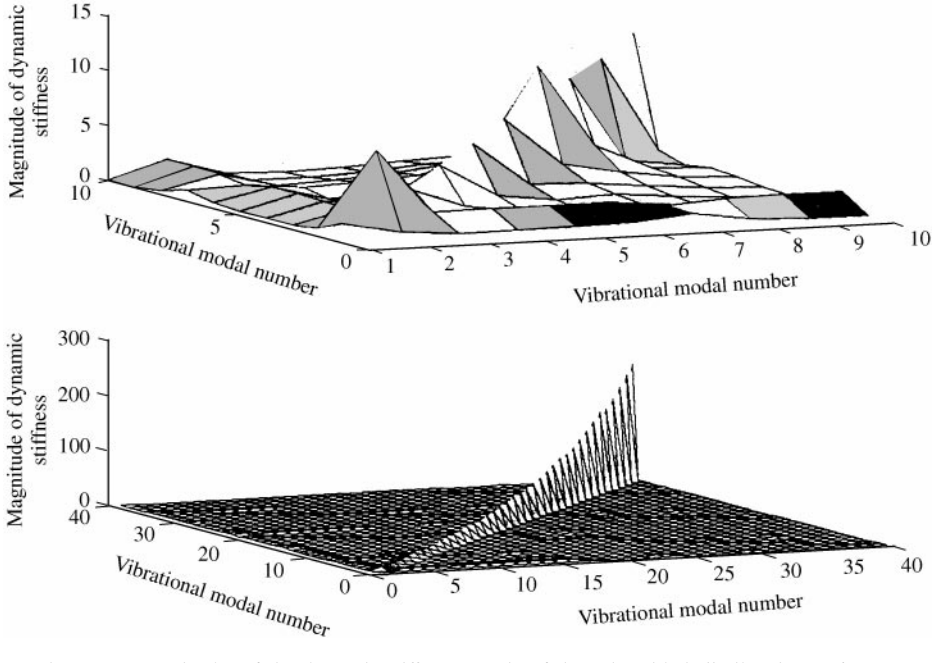

Figure 4. Magnitudes of the dynamic stiffness matrix of the spheroid shell vibration at $ka = 1{\cdot}8$.

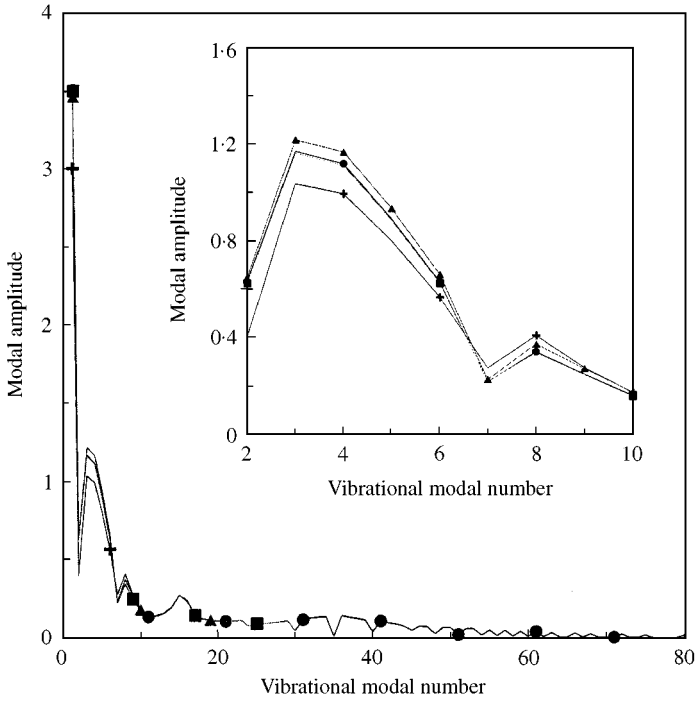

Figure 5. The vibrational modal amplitudes solved by using 10, 20, 30 and 80 vibrating modes for forming equation (15). —●—, 80 modes; —+—, 10 modes; —▲—, 20 modes; —■—, 30 modes.

The convergence of the amplitudes can be examined from Figure 4. The magnitudes of the dynamic stiffnesses, which include the acoustic impedances, exhibit a diagonal-dominated feature in which the influence of the cross-impedances becomes less important with ascending mode numbers. This feature indicates that the low order vibrational modes are coupled together due to the cross-impedances and the higher order modes become independent. According to equation (15), the equation of motion of the ith modal amplitude q_i is

$$\frac{\rho_s}{\rho_0}\frac{h_0}{a}[-(ka)^2+(k_ia)^2]q_i+(-\mathrm{i}ka)\sum_{j=1}^{N_s}Z_{ij}q_j=\hat{f}_i. \tag{21}$$

To examine how the cross-impedances affect the solved amplitudes, we consider the ratio r_{ij} of the off-diagonal terms Z_{ij}, $i \neq j$, to the diagonal term of the above equation

$$r_{ij}=\left|\frac{(-\mathrm{i}ka)Z_{ij}}{\rho_s/\rho_0\,(h_0/a)[-(ka)^2+(k_ia)^2]+(-\mathrm{i}ka)Z_{ii}}.\right| \tag{22}$$

where "| |" denotes magnitude of complex values. The ratio r_{ij} refers to the coupling tendency of the mode j to the mode i. A small value of r_{ij} implies that the effect of the mode j to the mode i is less important. Figure 4 implies that for a large i, the ratio of r_{ij} for $i \neq j$ becomes very small. Therefore, the equation of large order modal amplitude q_i becomes diagonal so that the amplitude q_i is

$$q_i=\frac{\hat{f}_i}{\rho_s/\rho_0\,(h_0/a)[-(ka)^2+(k_ia)^2]+(-\mathrm{i}ka)Z_{ii}}. \tag{23}$$

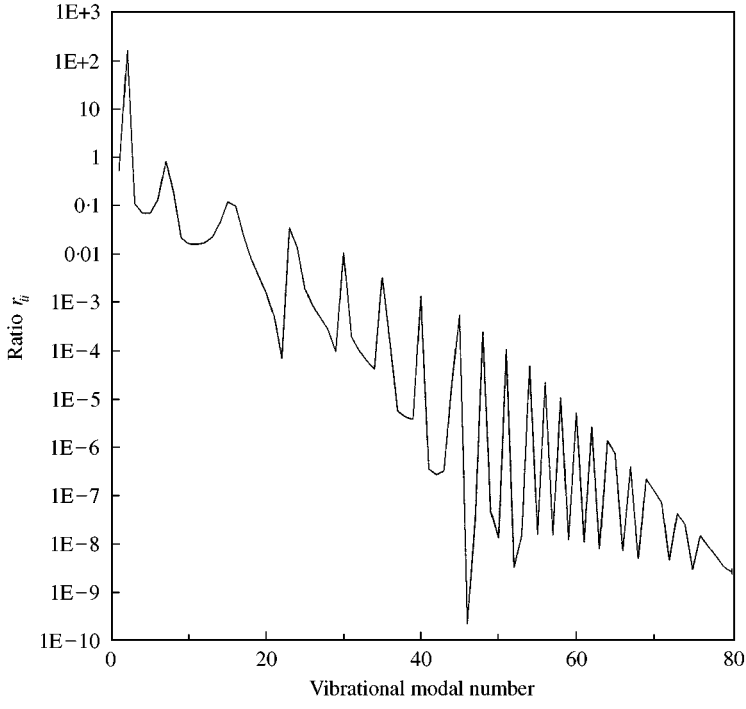

Figure 6. The dependence of the ratio r_{ii} on the vibrational modal number for $ka = 1{\cdot}8$.

which indicates that those modes react independently with other modes. Moreover, since the cross-impedances are smaller than self-impedances (Figure 2), the ratio r_{ij} has the following inequality:

$$r_{ij} \leqslant r_{ii}. \tag{24}$$

Consequently, the ratio of r_{ii} can be an indicator of the degree to which a vibration modal amplitude q_i couples with other modes. Thus, the solution of the coupled equation, equation (15), is divided into two categories: the modes coupled together due to comparable amounts of acoustic cross-impedance loadings to the structural modal mass and stiffness effects, and the modes reacting independently for small values of r_{ii}. Figure 6 shows the ratio r_{ii} versus mode number, having small values for the high order vibrational modes. The equation of coupled modes for which the coefficients r_{ij} are finite values is obtained from equation (15) by maintaining the corresponding lower order mode coefficients of $[\Lambda]$ and $[Z]$. Let $\{q_c\}$ and $\{q_u\}$ be the modal amplitudes of coupled and uncoupled modes respectively. The corresponding partitioned equation of equation (15) thus becomes

$$\left(\begin{bmatrix} \Lambda_c & 0 \\ 0 & \Lambda_u \end{bmatrix} + (-\mathrm{i}ka) \begin{bmatrix} Z_{cc} & Z_{cu} \\ Z_{uc} & Z_{uu} \end{bmatrix} \right) \begin{Bmatrix} q_c \\ q_u \end{Bmatrix} = \begin{Bmatrix} \hat{f}_c \\ \hat{f}_u \end{Bmatrix}, \tag{25}$$

where the subscripts "c" and "u" denote the groups pertaining to coupled and uncoupled modes. The above second sub-matrix equation is a nearly diagonal matrix equation since the ratios of off-diagonal terms are very small for high order modes (see equations (21) and (23), and Figure 6). The uncoupled amplitudes $\{q_u\}$ can be approximated by equation (22).

Rewrite the first sub-equation as

$$([\Lambda_c] + (-\mathrm{i}ka)[Z_{cc}])\{q_c\} = \hat{f}_c - (-\mathrm{i}ka)Z_{cu}\{q_u\}, \tag{26}$$

in which the second term of the right-hand side of the above equation represents the coupling effect of the high order uncoupled modes to the low order coupled modes. However, the coupling effect is negligible if one replaces $\{q_u\}$ in the above equation with equation (22) so that the contribution of the coupling effect is of the order of r_{ij}, which is only a slight amount for large indexes i and j. This not only makes the higher order modes to become uncoupled, but also leads to a situation in which the solved amplitudes of a reduced equation, which is the equation obtained by retaining only the coupled modes, are approximately equal to the ones obtained by equation (15) without partitioning. The computed amplitudes in Figure 5 show that the amplitudes are convergent for employing modes more than 20. The corresponding r_{ii} value in Figure 6 for 20 truncated natural modes is approximately 0·01. This observation enables us to study the convergence of modal truncation for the expansion used in equation (1) for the errors arising in the surface response as well as the farfield solution.

5. CONVERGENCE OF SURFACE AND FARFIELD SOLUTIONS

The normal displacement can be computed by the solved amplitudes $\{q\}$ from equation (2), and the corresponding surface pressure is obtained using equation (9). Figures 7 and 8 present the dimensionless normal displacement and surface pressure along the arclength of

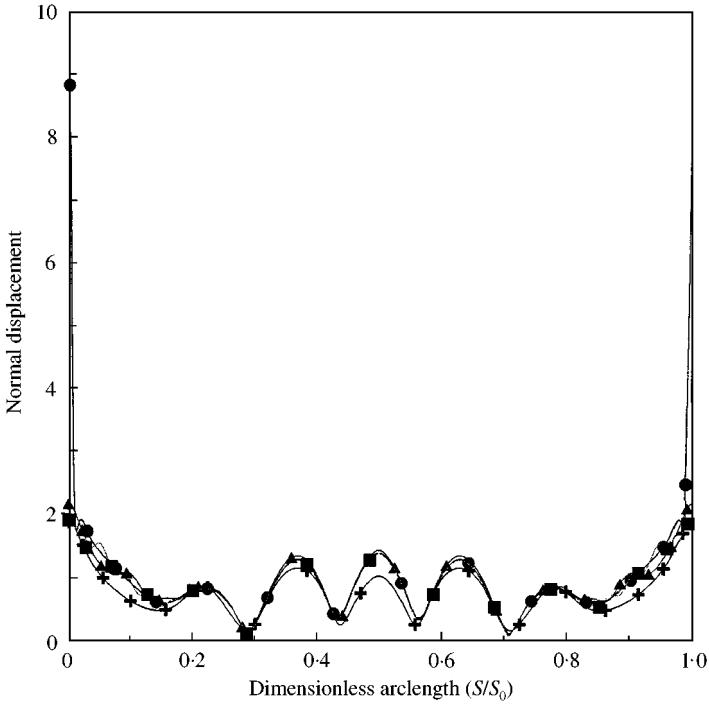

Figure 7. Magnitudes of normal displacements for $ka = 1{\cdot}8$ obtained by the solved vibrational modal amplitudes using 10, 20, 30, and 80 expansion natural models; —●—, 80 modes; —+—, 10 modes; —▲—, 20 modes; —■—, 30 modes.

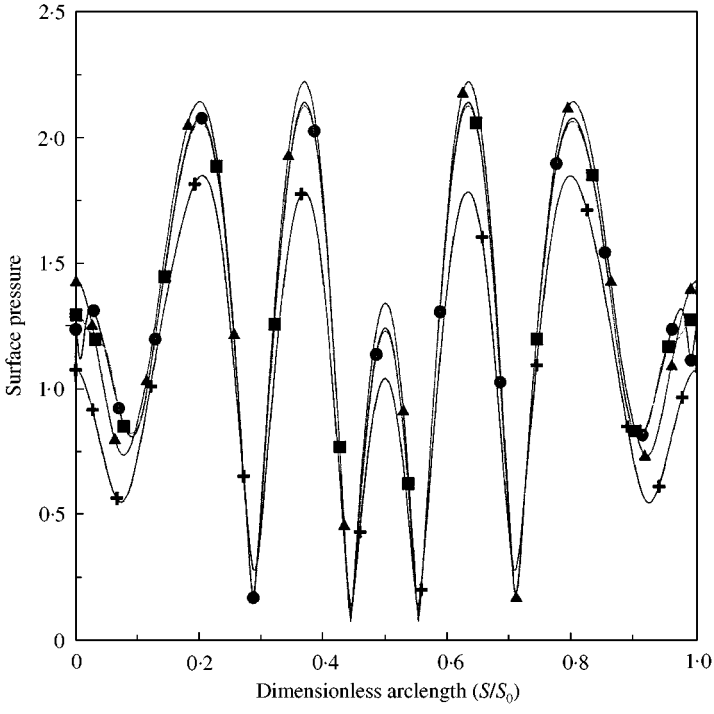

Figure 8. Magnitudes of surface pressure obtained for $ka = 1{\cdot}8$ by equation (9) using 10, 20, 30, and 80 expansion natural modes; —●—, 80 modes; —+—, 10 modes; —▲—, 20 modes; —■—, 30 modes.

a generator of the spheroid, where the displacement and surface pressure are divided by the minor axis a and by $\rho_0 c_0^2$ respectively. In the figures, the dimensionless arclength is defined as the ratio of the arclength from one apex to the total arclength. The expansion modes are 10, 20, 30, and 80 modes respectively. The symbol S in these figures denotes the arclength from one of the apexes and S_0 is the total arc length of the generator. Some minor discrepancies occur when using various number modes, particularly near the regions of apexes. The factor $\sum_{i=1}^{N} (-\mathrm{i}ka)\, q_i \beta_{ij}$ in equation (8) represents modal amplitude corresponding to the radiation mode Φ_i. Let v_j denote the amplitude,

$$v_j = \sum_{i=1}^{N_s} (-\mathrm{i}ka) q_i \beta_{ij}. \tag{27}$$

Correspondingly, the pressure radiation modal amplitude is obtained by multiplying a phase shift factor $\lambda_j - \mathrm{i}/\sqrt{\lambda_j^2 + 1}$ by v_j [8]. A previous study [7] has indicated that the surface complex power of a vibrating surface can be identified as

$$P = \frac{1}{2} \sum_{j=1}^{N_f} \lambda_j |v_j|^2 - \frac{1}{2} \mathrm{i} \sum_{j=1}^{N_f} |v_j|^2, \tag{28}$$

where the real and imaginary parts are the radiated and reactive powers respectively. Equation (27) indicates that only the radiation modes whose eigenvalues are not zero contribute to the radiated power. Figure 9 displays the amplitudes v_j computed by equation (26) for the various natural number modes of 10, 20, 30, and 80 vibrational modes used in

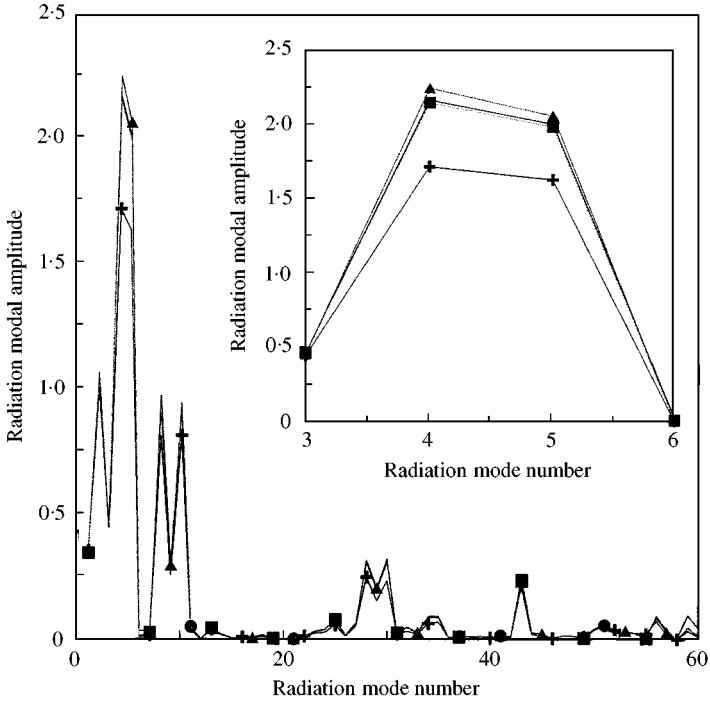

Figure 9. Magnitudes of radiation modal amplitudes computed by equation (26) using 10, 20, 30, and 80 expansion natural modes; —●—, 80 modes; —+—, 10 modes; —▲—, 20 modes; —■—, 30 modes.

the expansions. This figure reveals that radiation modal amplitudes computed by 20, 30 and 80 natural modes are generally identical, while some discrepancies occur for 10 expansion natural modes. The radiation modes within the fifth mode are strong radiators as stated previously, whose eigenvalues are not zero, causing effective radiations to the far field indicated by equation (27). Consequently, the erroneous predication of the radiation modal amplitudes q_i for using 10 natural modes leads to an error at the far field. The solution at the far field can be obtained by computing radiation patterns, which are obtained from factoring out a simple source term e^{ikr_r}, where r is the distance of the farfield point from the origin. Figure 10 illustrates the farfield radiation patterns, of which, the pattern obtained by 10 modes is different from the patterns of 20, 30 and 80 modes. The vertical axis in this figure corresponds to the symmetric axis of the spheroidal body.

This example illustrates that the number of natural modes employed in equation (15) for obtaining an accurate solution at the farfield depends on the convergence of velocity radiation modal amplitudes computed by equation (26). However, the number of natural modes necessarily used in equation (15), to make the solved amplitudes q_i convergent, is determined by the ratio r_{ii} such that a small value of r_{ii} implies that the modes beyond the ith natural mode are decoupled, which does not influence the solution of the modes below the ith mode. This situation is depicted in Figure 5 indicating that when more than 20 modes are selected, the resulting amplitudes are virtually the same. The ratio r_{ii} which corresponds to the 20th mode is approximately to be 0·01. A strictly convergent answer is required to use natural modes for amplitudes approaching zero, which is nearly 80 modes in this example. However, using 20 natural modes still provides a convergent answer at the farfield (see Figure 10) and a good enough one at the surface (see Figures 7 and 8). Another case for a vibrating frequency ka of 3·5 is also presented. Figure 11 plots the ratio r_{ii} versus

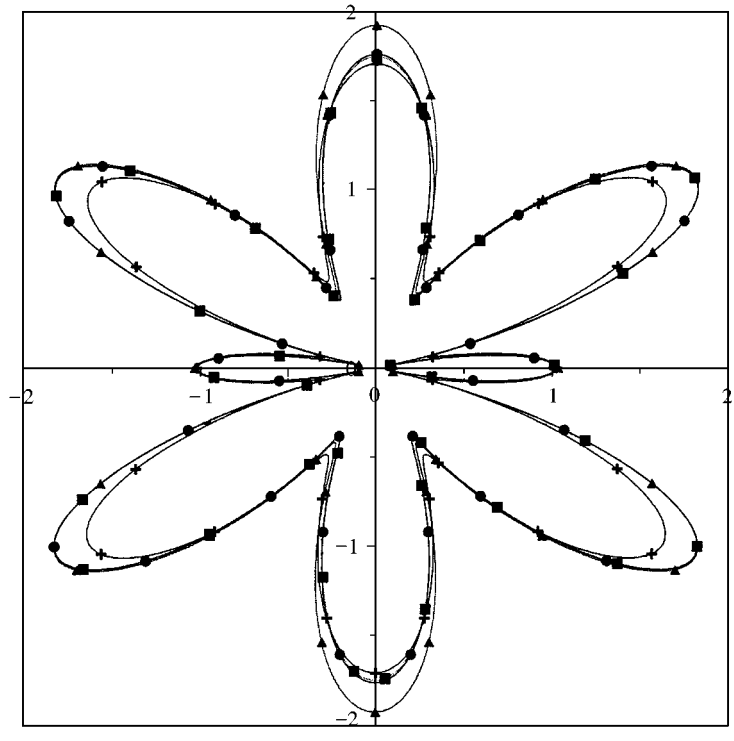

Figure 10. Radiation patterns for $ka = 1{\cdot}8$ obtained by using 10, 20, 30, and 80 expansion natural modes; —●—, 80 modes; —+—, 10 modes; —▲—, 20 modes; —■—, 30 modes.

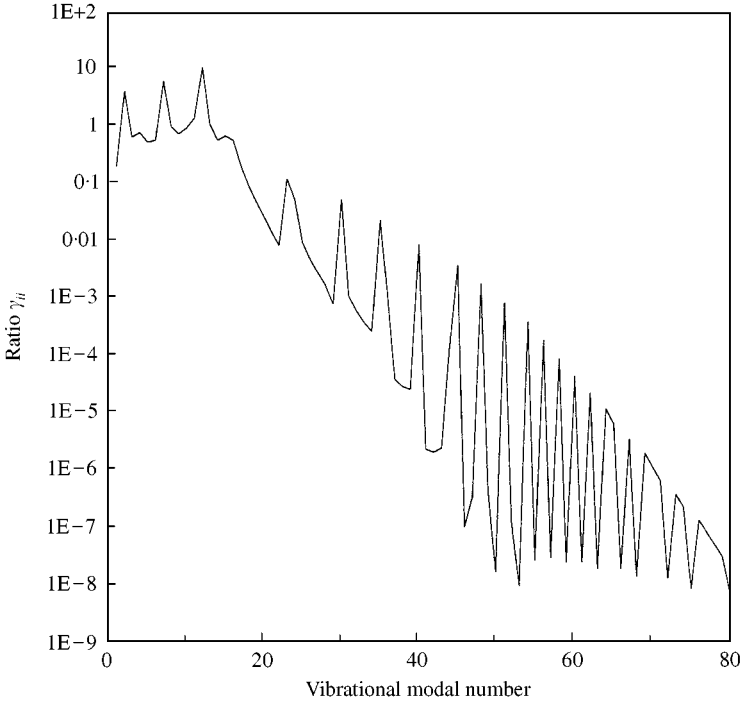

Figure 11. The dependence of the ratio r_{ii} on the vibrational modal number for $ka = 3{\cdot}5$.

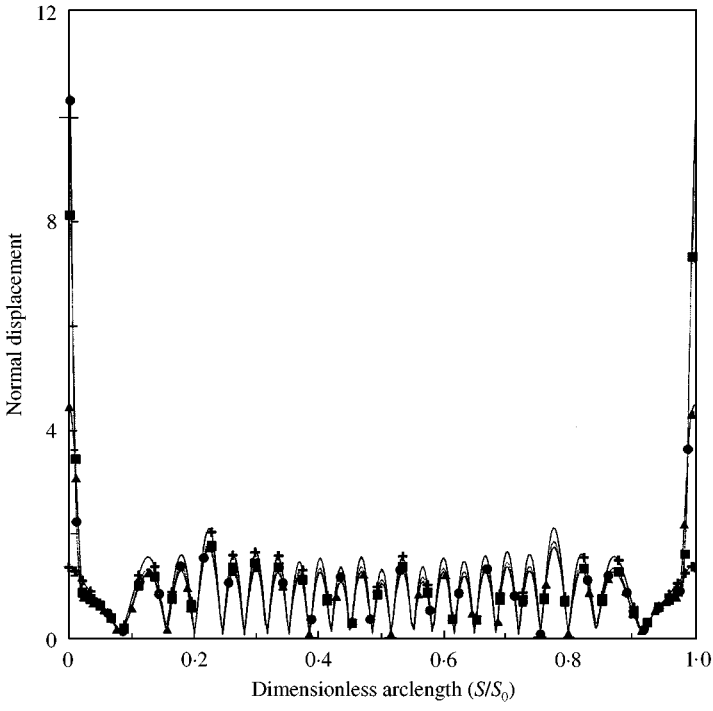

Figure 12. Magnitudes of normal displacements for $ka = 3{\cdot}5$ obtained by the solved vibrational modal amplitudes using 20, 40, 60, and 80 expansion natural modes; —●—, 80 modes; —+—, 20 modes; —▲—, 40 modes; —■—, 60 modes.

vibrational modal number. The value of r_{ii} for the 40th mode is approximately 0·01. According to the previous observations, using mode numbers beyond 40 would yield acceptable answers at the surface and convergent results at the far field. Figures 12 and 13 display the normal displacement and surface pressure, respectively, indicating that the results of using 20 modes present more discrepancy than that using 40, 60 and 80 modes, whereas using 80 modes provides convergent answers for the natural modal amplitudes approaching zero for high order modes. Accordingly, the farfield solution for using 20 modes displayed in Figure 14 shows obvious deviations from others. Finally, Figure 15 presents the radiation pattern spectrum of the farfield versus ka where the angle θ ranging from 0 to π is the polar angle defined in Figures 10 and 14, whose vertical axes corresponding to θ equal 0 and π. The plots show that maximum responses occur at ka around 1·5.

It would be instructive to comment on the convergent answers of the present analysis. A strict convergence refers to the expansion modal amplitudes $\{q\}$ in equation (15) approaching zero for high order nature modes. This requires much numerical effort due to the use of many terms of natural mode expansions (see the numerical example just demonstrated). A less expansive convergence can be regarded as the number of modes employed to have convergent answers at the farfield so that the coefficient of r_{ii} in equations (22) and (24) is very small (0·01 for the present example). The small value of r_{ii} makes the natural modes beyond the ith mode decouple from the acoustic loading, whose amplitudes are also small because the corresponding total dynamic stiffness effects due to the acoustic impedance loadings are very minor when compared with the dynamic stiffness attributed to the structure (see equations (22) and (23)). Consequently, one would

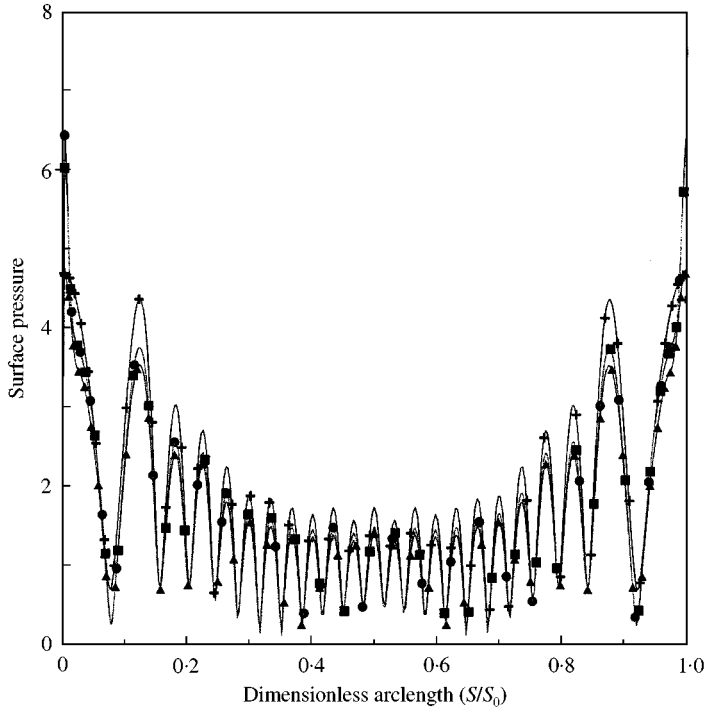

Figure 13. Magnitudes of surface pressure obtained for $ka = 3{\cdot}5$ by equation (9) for 20, 40, 60, and 80 expansion natural modes; —●—, 80 modes; —+—, 20 modes; —▲—, 40 modes; —■—, 60 modes.

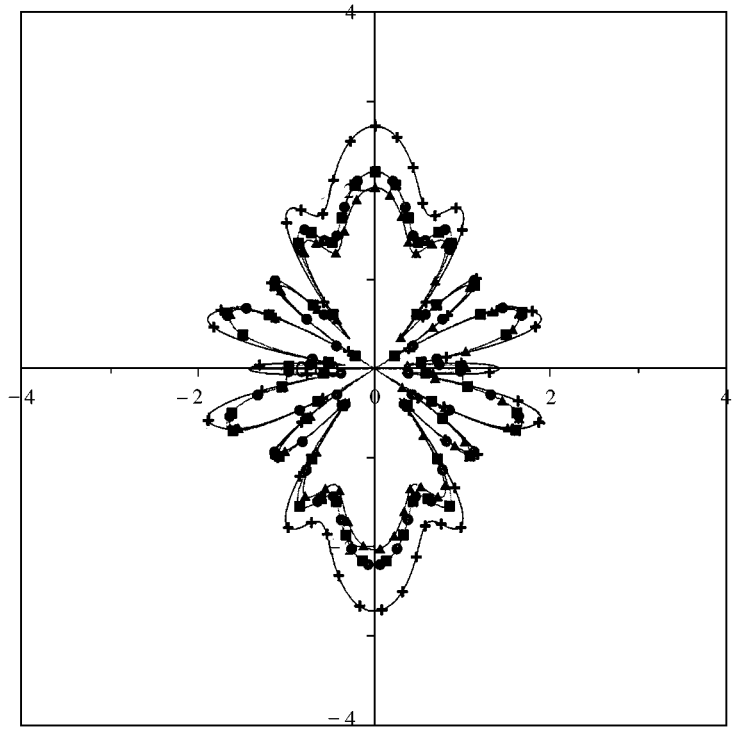

Figure 14. Radiation patterns for $ka = 3{\cdot}5$ obtained by using 20, 40, 60, and 80 expansion natural modes; —●—, 80 modes; —+—, 20 modes; —▲—, 40 modes; —■—, 60 modes.

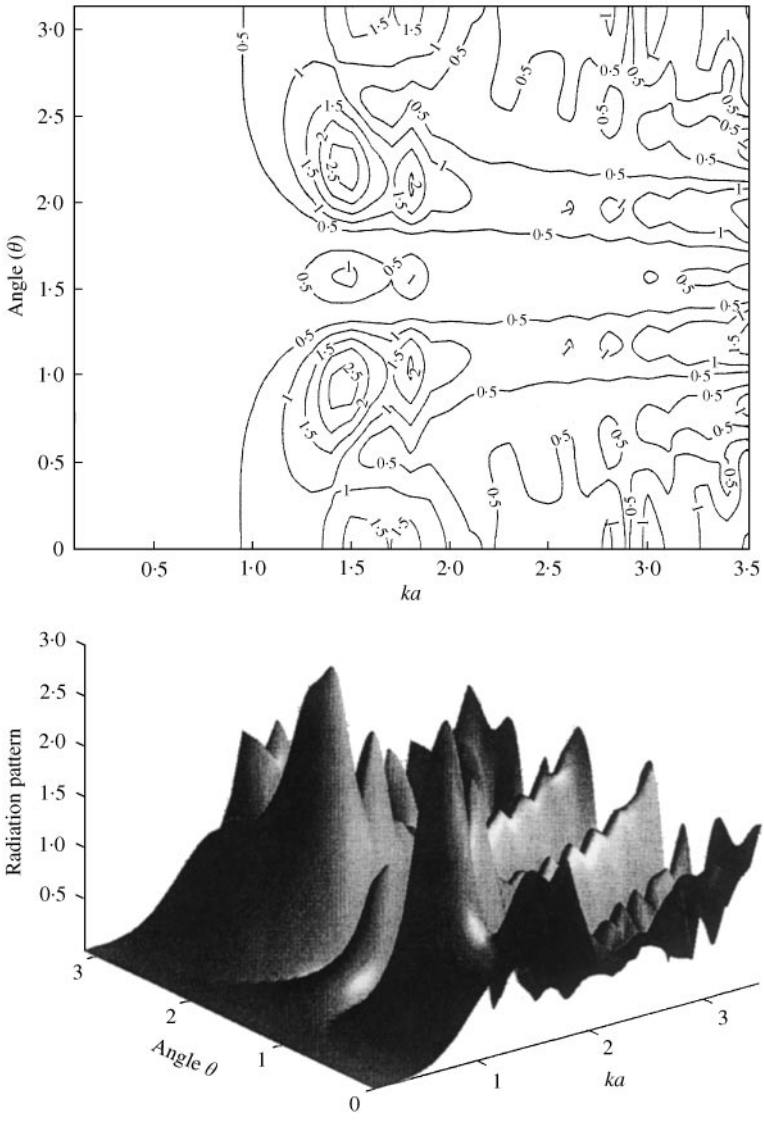

Figure 15. Spectrum of radiation pattern versus *ka*.

obtain acceptable answers for surface solutions and good convergent answers for farfield solutions.

6. CONCLUSIONS

The work presents a novel formulation for submerged structures using natural vibrational mode expansions to analyze the structural responses and acoustic radiations. The acoustic loading on the structures is derived as modal radiation impedances where the surface pressure and normal velocity are related to each other using radiation mode theory. In addition, the surface pressure and normal velocity are expanded by pressure and velocity

radiation modes, respectively, where a bi-orthogonal condition computes the expansion coefficients for pressure and velocity. These two amplitudes of the pressure and velocity have equal magnitude and phase shifts between them, which are determined by the associated eigenvalues of the radiation modes. Correspondingly, a symmetric impedance matrix is derived to describe the acoustic loading. The impedance matrix presents a self-impedance dominating feature, namely that the self-impedances associated with the vibrational modes are generally larger than the cross-impedances. The magnitudes of the impedances decrease with ascending mode numbers while the corresponding phases approach 90°. The equation of the submerged structures is formed when the structural modal dynamic stiffnesses are added to the acoustic impedances producing a time-derivative factor. The coupled equation for the structural–acoustic system can be partitioned in such a manner that the natural vibrational modes are categorized into coupled and uncoupled modes, based on the ratios of self-impedances to the diagonal terms of the coupled equation. Moreover, the surface response and farfield pressure are obtained by the solved modal amplitudes of the equation. The convergence of surface responses is justified the solved amplitudes by approaching zero, while the farfield pressure is convergent when the corresponding strong velocity modes are convergent. The weak radiation modal amplitudes do not necessarily converge because the weak radiators only produce evanescent fields. The present formulation provides an effective means of analyzing the coupling of vibrational modes for the submerged structures and the convergence of near and farfield solutions in relation to acoustic radiation modes.

ACKNOWLEDGMENTS

The authors would like to thank the National Science Council of the Republic of China for financially supporting this research under Contract No. NSC-88-2611-E019.

REFERENCES

1. H. Huang and Y. F. Wang 1985 *Journal of the Acoustical Society of America* **77**, 1389–1394. Asymptotic fluid–structure interaction theories for acoustic radiation prediction.
2. B. E. Sandman 1976 *Journal of the Acoustical Society of America* **60**, 1256–1264. Fluid loading influence coefficients for a finite cylindrical shell.
3. A. Harrari and B. E. Sandman 1976 *Journal of the Acoustic Society of America* **60**, 117–128. Vibratory response of laminated cylindrical shells embedded in an acoustic fluid.
4. P. R. Stepanishen 1982 *Journal of the Acoustical Society of America* **71**, 818–823. Modal coupling in the vibration of fluid loaded cylindrical shells.
5. B. Laulagent and J. L. Guyader 1989 *Journal of Sound and Vibration* **131**, 397–415. Modal analysis of a shell's acoustic in light and heavy fluids.
6. S.-H. Choi, T. Igusa and J. D. Achenbach 1996 *Journal of Sound and Vibration* **197**, 329–350. Acoustic radiation from a finite-length shell with non-axisymmetric substructures using a surface variational principle.
7. P. T. Chen 1997 *Journal of Sound and Vibration* **208**, 55–71. Vibrations of submerged structures in a heavy acoustic medium using radiation modes.
8. P. T. Chen and J. H. Ginsberg 1995 *Journal of the Acoustical Society of America* **98**, 3343–3351. Complex power, reciprocity, and radiation modes for submerged bodies.
9. P. T. Chen and J. H. Ginsberg 1992 *Journal of the Acoustical Society of America* **92**, 1499–1508. Modal properties and eigenvalue veering phenomena in axisymmetric vibration of spheroidal shells.
10. A. D. Pierce 1981 *Acoustics, An Introduction to its Physical Principles and Application*. New York: McGraw-Hill; chapio.

APPENDIX A: NOMENCLATURE

T	kinetic energy of shell equations
V	potential energy of shell equations
N_s	the number of expanded natural modes
N_f	the number of expanded radiation modes
E	Young's modulus of the shell structures
h_0	thickness of the shells
a	radius of minor axis of the spheroidal shells
ρ_s	density of the shells material
$\Delta_i a$	non-dimensionalized natural frequencies of the shells
Δ_i	$\Delta_i = \Omega_i / c_0$
Ω_i	circular natural frequencies of the shells
c_d	dilatational wave speed of the shell material ($c_d = (E/\rho_s)^{1/2}$)
c_0	sound speed of the fluid
q_i	modal amplitude coefficient for the natural mode expansions
w_n	normal displacement of the shell surfaces
δW	virtual work done by surface pressure and an external point force
f_0	an external point force
$\phi_{n,i}$	normal displacement of the ith natural mode, the subscript "n" referring to the normal direction
$\phi^*_{n,i}$	the normal displacement value at the location of the applied external force
ρ_0	density of the fluid
p	dimensionless surface pressure, which is defined as the pressure divided by $\rho_0 c_0^2$, similar definition for the pressure variables
p_i	dimensionless surface pressure due to the normal velocity of ith natural mode $\phi_{n,i}$
k	acoustic wave number ($k = \omega / c_0$)
ω	circular vibrating frequency
β_{ij}	expansion coefficient of the normal displacement of the ith natural mode in terms of the jth radiation modes
N_f	the number of expanded surface acoustic radiation modes
Φ_i	velocity radiation mode
Ψ_i	pressure radiation mode
δ_{ij}	Kroneck delta symbol
λ_i	eigenvalue of the radiation mode
f_ℓ	generalized force of the point force f_0 associated with the ℓth natural mode
$\hat{f}_\ell$	dimensionless generalized force
$[\Lambda]$	a diagonal matrix defining the dynamic stiffness in terms of natural mode expansions
$[Z]$	complex impedance matrix
P_{ij}	dimensionless acoustic power attributed to the self-impedance of the ith natural mode
$P_{i\ell}$	dimensionless complex acoustic power arisen from the cross-coupling impedance due to the ith and ℓth natural modes
r_{ij}	coefficient defining the coupling tendency of the ith and jth natural modes
P	dimensionless complex surface acoustic power by a vibrating surface